catalysts

MDPI

Article

Conversion of Carbon Monoxide into Methanol on Alumina-Supported Cobalt Catalyst: Role of the Support and Reaction Mechanism—A Theoretical Study

Nguyen Ngoc Ha, Nguyen Thi Thu Ha, Nguyen Binh Long and Le Minh Cam *

Faculty of Chemistry, Hanoi National University of Education, Ha Noi 100000, Vietnam; hann@hnue.edu.vn (N.N.H.); ntt.ha@hnue.edu.vn (N.T.T.H.); binhlongsonla@gmail.com (N.B.L.)

* Correspondence: camlm@hnue.edu.vn; Tel.: +84-989-886-242

Received: 12 November 2018; Accepted: 19 December 2018; Published: 23 December 2018

Abstract: Density functional theory (DFT) was used to calculate the step-by-step hydrogenation of carbon monoxide (CO) to form methanol over a Co_4 cluster/Al_2O_3 surface. A three-dimensional Co_4 tetrahedral structure was selected to explore its interaction with the supporting Al_2O_3 (104) surface. Co_4 chemically reacted with Al_2O_3 to form a new chemical system. The calculated results show that Al_2O_3 support has strengthened the Co_4 catalyst during the reaction since the formation of the Co–O bond. Loading Co_4 on the Al_2O_3 surface increases CO adsorption ability but decreases the dissociation ability of C–O to produce hydrocarbons. As such, CH_3OH formation becomes more favorable both kinetically and thermodynamically on Co_4/Al_2O_3. In CO hydrogenation, methanol was synthesized through a CO reaction with hydrogen via either an Eley–Rideal or Langmuir–Hinshelwood pathway to form the intermediates C*-O-H, H-C*-OH, H_2-C*-OH, and finally the hydrogenation of H_2-C*-OH to methanol with both hydrogenation steps forming C*-OH and final product as rate-limiting. These results showed that the interaction between Co, Al_2O_3 and H_2 pressure can change the pathway of CO hydrogenation on Co/Al_2O_3 and it may, therefore, influence distribution of the final products.

Keywords: density functional theory; Co_4 cluster; Al_2O_3; support; adsorption; mechanism; methanol

1. Introduction

Methanol synthesis by carbon monoxide (CO) and carbon dioxide (CO_2) hydrogenation has been widely studied both experimentally and theoretically [1–6] because methanol is an important raw material of crucial importance in the chemical and energy industries.

In recent years oxide-supported metal catalysts have been extensively studied for CO hydrogenation to methanol such as modified catalysts of the Fischer–Tropsch process or Cu-based catalysts [7–12], Mo-based catalysts [13–16], and cobalt nanoparticles [17–20]. However, the methanol selectivity and catalytic stability remain rather poor. Thus, the development of a good catalyst with high selectivity and stability is required. In order to improve the methanol yield, many efforts have been made to understand the reaction mechanism and to suggest different reaction pathways to gain methanol via hydrogenation of CO and CO_2.

Many studies have been devoted to the reaction mechanism over catalysts, controversies still remain. In the work done by Li et al. [21] a reaction mechanism on the transition metal (Fe, Co or Ni) promoted MoS_2- based catalyst was proposed. Different reaction pathways on different catalytic phases (MS_x and M-KMoS) were suggested. On the MS_x phase, CO dissociates and is subsequently hydrogenated into CH_x and methane while on the mixed M-KMoS phase non-dissociative adsorbed

CO inserts into a metal–methyl carbon bond producing an oxygenate precursor, which upon further hydrogenation or dehydration forms mixed C^{2+} oxygenates and hydrocarbons.

CO hydrogenation on these two MoS_2 (10-10) surfaces was also investigated by Shi et al. [22] using density functional theory (DFT) calculations. Their results show that the route for the CO hydrogenation is the following:

$$CO + H \rightarrow HCO$$

$$HCO + H \rightarrow H_2CO$$

$$H_2CO + H \rightarrow H_2COH$$

$$H_2COH \rightarrow OH + CH_2$$

$$CH_2 + H \rightarrow CH_3$$

$$CH_3 + H \rightarrow CH_4$$

Studt et al. [11] proposed that the hydrogenation of CO occurs at the carbon end of adsorbed CO. Firstly, HCO is formed following by H_2CO and finally to H_3CO. The last step in the reaction cascade to yield methanol is the hydrogenation of methoxy. Meanwhile, the hydrogenation of the oxygen end generating COH, HCOH and H_2COH intermediates possessed much higher barriers and all intermediates have higher energy than their carbon hydrogenated counterparts

Besides controversy about the mechanism, there is also no general agreement in the nature of the active site(s) and the effect of oxide support. It has been well established that due to the strong metal–support interactions a support can remarkable affect the active metal dispersion, reducibility, which then have an important influence on the catalytic activity [23]. Ramírez et al. [23] who studied the behavior of cobalt-based catalysts supported on several metal oxides in the CO_2 methanation reaction at atmospheric pressure and low temperatures (200–300 °C) found that apart from the Co particle size and oxidation state of active species, the catalytic activity and selectivity can also be affected by the nature of the support. Zuo et al. [24] suggested while hydrogenation of CO over metallic Cu does not generate methanol, the methanol can be synthesized from CO hydrogenation over Cu/ZnO due to a strong synergetic interaction between metallic Cu and the oxide support ZnO. In the work done by Lee et al. [25] the effect of the support and the interaction of Cu species with different supports were studied. The authors indicated that over zinc supported catalysts a higher conversion (70%) and selectivity towards higher alcohols (70%) were obtained. However, Medford et al. [26] indicated that the reaction was inhibited by the presence of very low CO_2 concentration.

γ-Al_2O_3 is the most common inorganic oxide which is used as a support since its excellent thermal stability, fine particle size, high surface area and wide range of chemical, physical, and catalytic properties. In the work of Prasad et al. [27], iron-based catalysts dispersed on different supports have been extensively investigated. Among studied supports, the performance of γ-Al_2O_3 is best, followed by silicas and titanias. The good performance of may be attributed to the strong metal-support interaction, which results in well dispersed catalyst and hinders catalyst sintering. Reuel et al. [28] studied 10 wt.% Co catalysts supported on MgO, carbon, SiO_2 and Al_2O_3. They found that the specific activity in the hydrogenation of carbon monoxide depends on the nature of the support in the following order: MgO < carbon < SiO_2< Al_2O_3.

Theoretically, the mechanism and reaction pathways of CO hydrogenation are also extensively studied. Recently, theory has been recognized as an important tool in the design and optimization of catalysts for many applications [29,30]. Among theoretical methods used to study the electronic configurations and properties of many-body systems, in particular catalytic reactions, DFT is known as a versatile and effective method. The fundamental aspect of the DFT method is that the characteristics of many-electron systems can be using the electron density which depends only on the three Cartesian variables. Using the DFT approach, computational accuracy can be significantly increased without the additional increase in the computational costs. Due to its advances, DFT can simulate catalytic

process at surfaces with the detail and accuracy required for calculated results to compare with experiments [31]. This understanding allows theoretical optimization for better catalysts.

Using periodic DFT calculations Andersen et al. [15] investigated the influence of K-doping on MoS_2 activity in the CO hydrogenation. They found that doping K created K-O and K-C bonding on the MoS_2 surface and hence enhanced the CO adsorption. The DFT calculations show that K-doping promotes the formation of mixed higher C_{2+} oxygenates. Reimers et al. [30] studied theoretically the catalytic activities of Zn, Ce and Ga oxides in the consecutive hydrogenation reactions of the CO molecule. Their calculated results indicated that the methanol formation proceeds via formyl (HCO), followed by the formation of formaldehyde (H_2CO), then methoxy (H_3CO) and, finally, methanol.

In the study of Studt et al. [11] DFT results revealed that over Cu (211) the CO hydrogenation occurs at the carbon end of adsorbed CO and the formation of methanol is processed through HCO, H_2CO, H_3CO intermediates. In contrast, hydrogenation at the oxygen end will process via COH, HCOH and H_2COH intermediates with much higher barriers.

A DFT study has been conducted by Dou et al. [32] to study the effect of ZrO_2 support on the catalytic behavior of In_2O_3 in the methanol synthesis from CO_2 and CO hydrogenation. The calculations show that ZrO_2 has a significant influence on the suppression of the dissociation of CO_2 and stabilization of H_2COO species on the surface of In_2O_3 catalyst.

The hydrogenation and dissociation reaction network of carbon monoxide (CO) over a Co-doped Cu (111) surface were theoretically studied using DFT. The calculated results revealed that the H-assisted route proceeds with the formation of HCO, CH_2O and CH_3O while OH-assisted route proceeds with the formation of COH, CHOH and CH_2OH [33].

The influence of surface hydroxyls over Ni/γ-Al_2O_3 and Cu/γ-Al_2O_3 has been investigated theoretically by Pan et al. [34] and Zhang et al. [35]. Their calculations show that the hydroxylation of γ-Al_2O_3 changes the reaction pathway and finally will influence the products distribution and hence, the process selectivity.

Zuo et al. [36] investigated theoretically the CO and CO_2 hydrogenation on Cu/γ-Al_2O_3 (110) surface in liquid paraffin. Their results indicated that the synthesis of methanol occurs via the formation of CHO, CH_2O, and CH_3O intermediates with CHO hydrogenation as the rate-limiting step.

With the above analysis, the objective in this work is to study the impact of the nature of the support on the physicochemical properties of Co-based catalyst and its activity in CO hydrogenation. We investigated the elementary steps resulting in the formation of methanol on Co/Al_2O_3 using the density functional theory (DFT) calculations. Co_4 cluster was chosen because Co_4 is the smallest cluster that possesses a three-dimensional structure and it could include both metal–metal and metal–support interactions. A model of Al_2O_3(104)-(2x2x2) based on X-ray diffraction (XRD) experimental results was adopted [37].

In our results, firstly we concentrate on the reactants adsorption and the configurations of the key intermediates involved in the process mechanism, followed by the energies.

2. Model and Computational Methods

In this study, a model of Al_2O_3(104)-(2x2x2) was selected based on the XRD experimental results [37]. Clusters of Co_4 in tetrahedral and rhombus forms were studied to select the stable structure.

The SIESTA (Spanish Initiative for Electronic Simulations with Thousands of Atoms) package based on the DFT approach was used for all geometry and energy calculations [38]. SIESTA has been successfully performed to study on the Fischer–Tropch reaction [39–41] due to its advantages in robust and accurate aspect.

The generalized gradient approximation (GGA) with the Perdew, Burke, and Ernzerhof (PBE) non-local gradient-corrected functional was employed to estimate the exchange correlation energy [42]. According to the large number of atoms in the studied systems (about 100 atoms), the double zeta basis plus polarization orbitals (DZP) was used for valence electrons, while the core electrons were treated using the norm-conserving pseudo potentials (NCP) in its fully non-local (Kleinman–Bylander)

form [43]. The Coulomb potential was expanded in a plane-wave basis with an energy cut-off of 150 Ryd. The systems were placed in boxes of 25×25×25 Å, which are big enough to have negligible electric fields at their edges. Spin-polarized calculations have been performed for all systems including metals. All equilibrium structures were obtained using the quasi-Newton algorithm, and the forces acting on the dynamic atoms all are smaller than 0.05 eV/Å.

When studying the step-by-step conversion of CO into methanol on the catalytic system, all the transition states were determined using a climbing image nudged elastic band (CI-NEB) method [44]. The advantages of the CI-NEB methods are that after the convergence is reached, the climbing image will converge to the saddle point and all the images occuring in the reaction coordinates are being relaxed simultaneously. In this work, the total number of images involved in the reaction path is seven, including the initial and the final configurations. In the CI-NEB calculations, the convergence tolerance is 0.1 eV/Å in the magnitude of the forces.

The energy variation is used as a significant criterion to predict the ability and the extent of all the processes. Additionally, to estimate the nature of the adsorbate and substrate interaction, a crucial change in the geometrical parameters was analyzed. Moreover, the atomic partial charges, estimated by means of the Voronoi deformation density (VDD) method, were reported. The VDD method avoids the problems inherent to basis set based schemes and provides meaningful charges that conform to chemical experience [45]. Moreover, the Mayer bond orders were also calculated. The Mayer bond orders are also less dependent on the basis of set choice and they are transferable and can be used to describe similar systems.

3. Results and Discussion

3.1. Electronic Properties of Co_4 and Co_4/Al_2O_3 Systems

Co_4 clusters were optimized in both tetrahedral and rhombus geometries (Figure 1). The calculated binding energies, E_b (E_b= [4E(M) – E(M_4)]/4) and the numbers of unpaired electrons, N_{ue} are presented in Table 1.

Figure 1. Tetrahedral (**a**) and rhombus (**b**) structures of Co_4 cluster; key distances are given in Å.

Table 1. The calculated binding energies (E_b, eV/atom), the numbers of unpaired electrons (N_{ue}) of Co_4 clusters.

Structure	E_b	N_{ue}
Tetrahedral	3.86	12
Rhombus	3.41	12

The calculated binding energy of the tetrahedral structure is higher than that of the rhombus. Hence, for Co_4 cluster the tetrahedral structure is more pronounced.

In our calculations, we have used collinear spin polarized option. The total spin polarization for the optimal structure were automatically determined corresponding to the structure with the lowest energy. Furthermore, the Co_4 structure were optimized with the fixed spin corresponding to the presence of 10 or 14 unpaired electrons. The results have confirmed that the Co_4 structure with 12 unpaired electrons is the most stable due to the lowest energy (see Supplementary, Table S1).

It is interesting to note that the Co atom has three unpaired electrons, while Co_4 has 12 unpaired electrons. Thus, the formation of Co_4 does not involve the electron pairing. In other words, metallic bonding is present even in clusters as small as Co_4. Moreover, the Co–Co bond lengths in tetrahedral and rhombus clusters are 2.521 and 2.520 Å, respectively which are shorter than twice the atomic radii of Co (1.35 Å, [46]). This again confirms the formation of chemical bonds between cobalt atoms in the cluster structures.

To evaluate the interaction between the clusters and the support, the initial cobalt clusters were placed at several positions on the surface of Al_2O_3 and the interaction energies were calculated (See Supplementary, Table S2). By comparing the interaction energy, the most stable structure of Co_4 on Al_2O_3 was found and is presented in Figure 2.

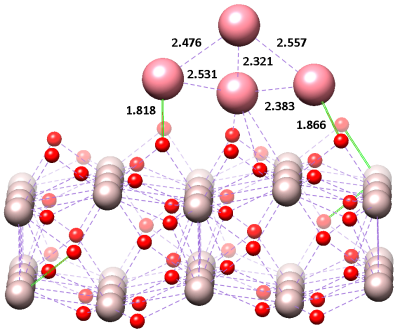

Figure 2. The optimized structure of Co_4/Al_2O_3 systems (colors: red—oxygen atom, grey—alumina atoms, violet—cobalt atoms); key distances are given in Å.

The structure of the Co_4 cluster on Al_2O_3 is close to the tetrahedron, the number of unpaired electrons of Co_4 has been reduced to 10 in comparison to the cluster alone. This is attributed to the partly transfer of electrons from the metal clusters to the alumina support. The total atomic charge of Co_4 cluster is calculated to be +0.944 which demonstrates the strong interaction between the cluster and the support. Moreover, the closest distance between Co and O atoms in Co_4/Al_2O_3 system (1.818 Å) is shorter than the sum of the atomic radius of Co and O atoms (1.95 Å [46]). Hence, the formation of Co_4/Al_2O_3 system is certainly accompanied by the formation of chemical bonds between Co and O atoms in Al_2O_3. The bonding formation is confirmed by the total Mayer bond order between Co and O, which is determined to be 1.712.

Due to the formation of chemical bonds the properties of Co_4/Al_2O_3 system are expected to differ from initial Co_4 cluster.

3.2. Adsorption of CO and H_2 on Co_4, Al_2O_3 and Co_4/Al_2O_3 Systems

3.2.1. Adsorption of CO on Co_4 and Co_4/Al_2O_3 Systems

The adsorption of CO on the catalytic systems plays an important role and mainly governs the formation of hydrogenation products. Therefore, a detailed study of the mechanism of this process is essential.

Adsorption of the CO molecule on transition metals can be defined in terms of donation of electron density from CO to the metal and π-back donation of electrons from filled *d* orbitals on the metal into vacant antibonding π^* orbitals on the CO [47]. Hence, CO is more favorably adsorbed via the C atom than the O atom. The calculated results also indicate that when a CO molecule is adsorbed on Co_4 and Co_4/Al_2O_3 systems the interaction of C–Co is always thermodynamically more favorable compared to the O–Co orientation (see Supplementary, Table S3). With the C–Co orientation, there are two possibilities for the CO adsorption: C atom in CO is bound to one Co atom (d-1 configuration); and C atom in CO is simultaneously bound to two Co atoms (d-2 configuration). The optimized configurations of CO adsorbed on Co_4 cluster and Co_4/Al_2O_3 system are presented in Table S3 of Supplementary.

The optimized structures of the d-1 and d-2 configurations for the CO adsorbed on Co_4/Al_2O_3 are illustrated in Figure 3. Table 2 summarizes the calculated results of CO adsorption on Co_4 and Co_4/Al_2O_3 systems.

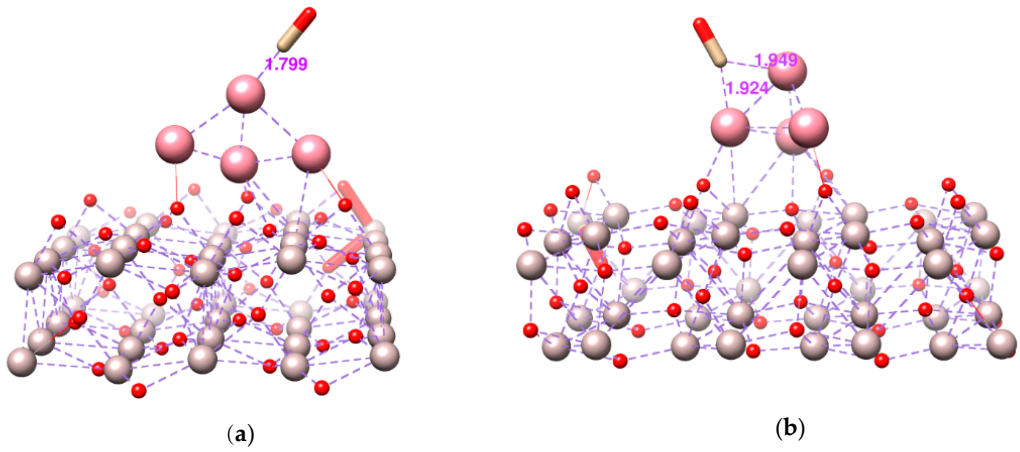

Figure 3. The optimized structure of the d-1 (**a**) and d-2 (**b**) configurations of CO-Co_4/Al_2O_3; (colors: red—oxygen atom, grey—alumina atoms, violet—cobalt atoms); key distances are given in Å.

Table 2. E_{ads} (in kJ mol^{-1}), $d_{C\text{-}O}$ (in Å) and bond-dissociation energy (BDE) of C–O (in kJ mol^{-1}).

Structures	d-1 Configuration			d-2 Configuration		
	E_{ads}	$d_{C\text{-}O}$	$BDE_{C\text{-}O}$	E_{ads}	$d_{C\text{-}O}$	$BDE_{C\text{-}O}$
Co_4	−186.9	1.172	960.6	−201.4	1.203	928.0
Co_4/Al_2O_3	−231.9	1.161	1004.3	−237.3	1.179	1023.5
CO		1.145	1190.3		1.145	1190.3
Exp.		1.128 [48]	1072 [49]			

From Table 2, one can see that when CO molecule is adsorbed on Co_4 cluster as well as on the Co_4/Al_2O_3 system, the weakness of C–O bond results in its elongation and the decrease of bond-dissociation energy. The adsorption energies of CO on Co_4/Al_2O_3 are lower than those on Co_4 cluster alone. These results indicate the role of the alumina support: the ***d-2*** configuration CO–Co_4/Al_2O_3 is the most favorable configuration due to the lowest adsorption energy, while the dissociation energy of the C–O bond in this configuration is highest. Thus, loading Co_4 on the Al_2O_3 surface leads to an increase in the CO adsorption ability but hinder the dissociation of C–O bond. In another words, hydrogenation of CO on Co_4/Al_2O_3 likely leads to the formation of oxygen-containing compounds. Notably, the adsorption of CO on Co_4/Al_2O_3 results in the formation of d-2 configuration. In this configuration the number of unpaired electrons is eight, while in the initial Co_4/Al_2O_3 system there are 10 unpaired electrons. Hence, two reduced electrons involve and to form a covalent bond between adsorbent and the CO molecule.

The obtained results regarding to the adsorption ability of CO on Co_4/Al_2O_3 show that Co_4/Al_2O_3 can catalyze the hydrogenation of CO into alcohols.

3.2.2. Adsorption of H_2 on Co_4 and Co_4/Al_2O_3 Systems

It has been established that for adsorption of hydrogen on the transition-metal surfaces the dissociative chemisorption is the preferred [50,51]. Our calculated results also revealthat H_2 dissociative adsorptions on Co_4 cluster and Co_4/Al_2O_3 system are favorable due to the lower adsorption energy (in comparison to that for molecular adsorption (see Supplementary, Table S4). The hydrogen adsorption on Co_4/Al_2O_3 releases 280.7 kJ mol^{-1}. The H–H distance is elongated from 0.776 Å (in the isolated molecule) to 3.145 Å (in the adsorption structure). Dissociated hydrogen atoms are simultaneously bound to two metal atoms on the surface of catalysts and thus will come to react with adsorbed CO molecule in the next reaction steps.

3.2.3. Adsorption of CO and H_2 on Al_2O_3 System

For comparison purposes, the adsorption of CO and H_2 on a pure Al_2O_3 support is also estimated. The calculations show that CO molecule is favorably adsorbed horizontally on the Al_2O_3 (104) surface at a distance of about 2.6 Å with an adsorption energy of −59.8 kJ mol^{-1}. The E_{ads} for H_2 adsorption on Al_2O_3 is −32.7 kJ mol^{-1} and the closest distance of H_2 to the Al_2O_3 surface is 2.3 Å (see Supplementary, Table S5) which reflects a physisorption in nature. These results indicate that Al_2O_3 can play a support role only. It interacts with the Co_4 sites to enhance the adsorption efficiency of Co toward CO and H_2.

3.3. Preliminary Investigation on the Process of CO Hydrogenation over Co_4/Al_2O_3 Catalyst to Methanol

We consider the first step in the CO conversion process to methanol, this step involves the interaction between CO and H_2 adsorbed molecules.

A schematic diagram of the suggested possible reaction pathway for the CH_3OH synthesis via the hydrogenation of CO on the Co_4/Al_2O_3 catalyst is presented in Figure 4a,b.

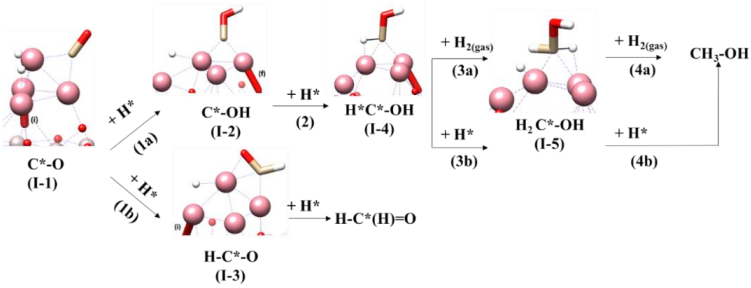

(**a**)

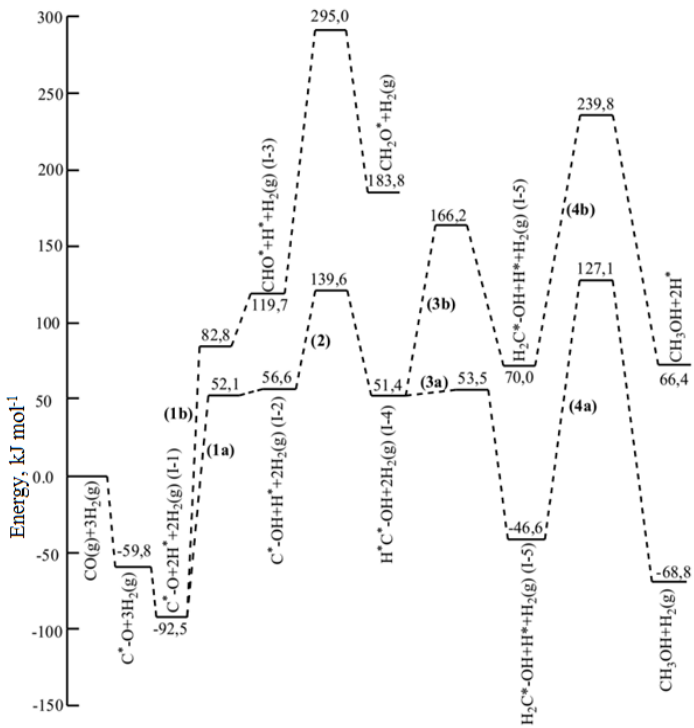

(**b**)

Figure 4. The possible reaction pathways for the CH_3OH synthesis via the hydrogenation of CO on the Co_4/Al_2O_3 catalyst (colors: bronze—carbon atom, red—oxygen atom, white—hydrogen atoms, violet—cobalt atoms), symbol "*" denotes the adsorbed species. Potential energy diagram obtained from density functional theory (DFT) calculations for CH_3OH synthesis via the hydrogenation of CO on the Co_4/Al_2O_3 catalyst, symbol "*" denotes the adsorbed species.

The reaction energy (ΔE) and the activation energy (E_a) of each stage are defined as:

$$E_a = E_{TS} - E_{IS}$$

$$\Delta E = E_{FS} - E_{IS}$$

where E_{TS}, E_{IS}, and E_{FS} are the total energies of the transition states (TS), the initial (IS) and final structures (FS), respectively.

The transition state structures of CO hydrogenation on Co_4/Al_2O_3 are presented in Table S6 of Supplementary. The calculated ΔE and E_a for each step are summarized in Table 3.

Table 3. The calculated ΔE and E_a for the CH_3OH synthesis reaction pathways.

Steps	ΔE (kJ mol^{-1})	E_a (kJ mol^{-1})
1a	149.10	144.6
1b	212.2	175.3
2	−5.2	83.0
3a	−97.8	2.1
3b	18.6	114.8
4a	−22.4	173.5
4b	47.8	221.2

Starting from the configuration I-1 with adsorbed CO and H species on the Co_4/Al_2O_3 surface (Figure 4a,b), the CO hydrogenation may firstly occur through two pathways: the adsorbed CO reacts with the neighboring adsorbed atomic H to generate the C*-OH (I-2) or H-C*-O (I-3) species (the asterisk denotes the adsorbed species). Optimized structures of I-1, I-2 and I-3 are presented in Figure 5. A comparison of the energies of formation (stability) and activation energies of COH and HCO formation by CO hydrogenation shows that the C*-O-H formation is energetically more favorable than H-C*=O formation. This finding is due to the lower activation energy (lower by 30.7 kJ mol^{-1}) and lower reaction energy (lower by 63.1 kJ mol^{-1}) of COH formation. Thus, CO hydrogenation is likely to proceed via the COH pathway. If one considered the I-3 configuration, the remaining adsorbed hydrogen atom H* may interact with the C atom of H-C*= O species to form formaldehyde –HC(H)=O.

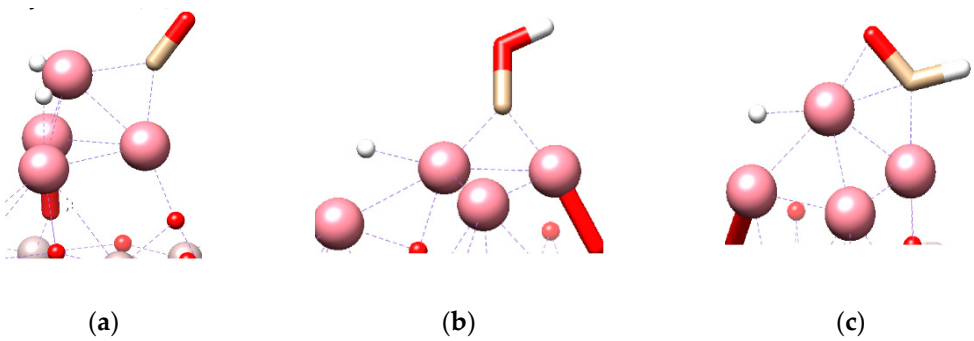

Figure 5. The optimized structures of I-1 (**a**), I-2 (**b**), and I-3 (**c**) (colors: brown—carbon atom, red—oxygen atom, white—hydrogen atoms, violet—cobalt atoms; symbols (i) and (f) denote the initial and final.

The formation of C*-O-H induced a remarkable change in the geometry of Co_4. The Co_4 tetrahedron is totally broken and a new Co_4 system is formed which is stabilized by the formation of new Co–O bond. The initial Co–O bond in I-1 structure (denoted as **i** in Figure 5) has been broken, a new Co–O (in Al_2O_3) bond is formed in I-2 structure (denoted as **f** in Figure 5) and there is no change in the Co–O bond in I-3 configuration. This change in structure of Co_4 can be attributed to the Al_2O_3 support, which stabilizes (strengthens) the Co_4 catalyst during the reaction due to the

formation of Co–O bonds. This stabilization may explain for the difference of our result in comparison to Zuo et al.'s calculation [36]. Zuo et al. study the CO hydrogenation over Cu_2 cluster adsorbs onto hydroxylated Al_2O_3 (110) surface in liquid paraffin. In their work, methanol was synthesized through the intermediate CHO rather than COH. Our calculation was based on a cluster of Co_4 adsorbed onto Al_2O_3 (104) surface. However, our finding is in agreement with the work done by Andersen et al. [15], who study CO hydrogenation over the MoS_2(100) surfaces using DFT calculations. Their results also indicated that the COH/HCOH route is more favorable than the HCO/H_2CO route on the Mo edge surface. The highest activation barrier in the COH/HCOH route is only 134.1 kJ mol^{-1}, which is lower than the barrier of 161.1 kJ mol^{-1} for the step forming HCO. These values agree well with our calculations.

From I-2, C*-OH is subsequently hydrogenated to form H-C*-OH (I-4) through interaction of one adsorbed hydrogen atom with C* of C*-OH:

$$H^* + C^*\text{-}OH \rightarrow H\text{-}C^*\text{-}OH$$

Energetically, this process is more dominated because it is exothermic with a negative reaction energy of ΔE (−5.2 kJ mol^{-1}). The activation energy is determined to be 83.0 kJ mol^{-1}.

Experimentally it is well know that at low hydrogen pressure the methanol formation follows the Langmuir–Hinshelwood mechanism, in which both reactants are adsorbed on the catalytic surface and the interactions between adsorbed species. However, at high hydrogen pressure, the reaction might occur via the Eley–Rideal mechanism, in which one reactant in gas phase will come to interact with other adsorbed reactant [14,52,53]. Based on this observation we predict two possible pathways to form methanol from H-C*-OH (I-4):

(i) In one route (steps 3a-4a), attack of hydrogen molecule from the gas phase with H-C*-OH (I-4) produces H_2C*-OH (I-5). This route is corresponding to the Eley–Rideal mechanism:

$$H_{2\,(gas)} + H\text{-}C^*\text{-}OH \rightarrow H_2C^*\text{-}OH + H^* \text{ (step 3a)}$$

The optimized structures of I-4 and I-5 are presented in Figure 6.

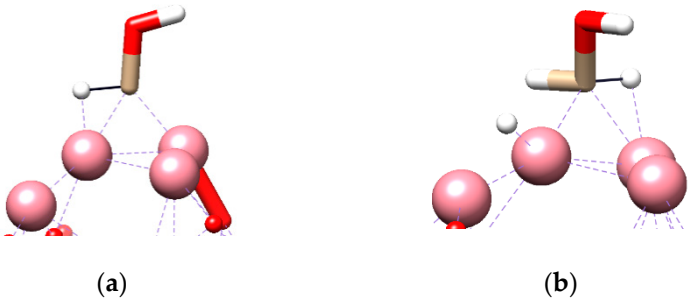

(**a**) (**b**)

Figure 6. The optimized structures of I-4 (**a**) and I-5 (**b**).

The formed H_2C*-OH (I-5) then subsequently undergoes hydrogenation by another H_2 from the gas phase producing H_3C*-OH and it will desorb to CH_3OH product (step 4a).

$$H_{2\,(gas)} + H_2\,C^*\text{-}OH \rightarrow H_3C^*\text{-}OH + H^* \rightarrow CH_3OH_{gas}$$

(ii) In the other route (3b-4b), one adsorbed hydrogen atom on the catalyst surface comes to combine with H-C*-OH (I-4) forming H_2C*-OH (I-5). The H_2C*-OH fragment further reacts with another adsorbed hydrogen atom and followed by desorption to release CH_3OH (step 4b). This route

is corresponding to the Langmuir–Hinshelwood mechanism and also has been suggested and calculated by several researchers [15,22,30,32]:

$$H^* + H\text{-}C^*\text{-}OH \rightarrow H_2C^*\text{-}OH \text{ (step 3b)}$$

$$H^* + H_2C^*\text{-}OH \rightarrow H_3C^*\text{-}OH \rightarrow CH_3OH_{gas} \text{ (step 4b)}$$

The formation of methanol by the direct attack of a hydrogen gas molecule to I-4 is energetically favorable because it is exothermic with a reaction energy of −97.8 kJ mol^{-1} and an activation energy of 2.1 kJ mol^{-1}. Meanwhile, the hydrogenation steps forming H_2C^*-OH and H_3C^*-OH through adsorbed hydrogen atoms are kinetically limited due to the higher activation barrier (114.8 kJ mol^{-1}).

These calculated results suggest that, at low pressure of H_2 and CO (meaning at low CO and H_2 surface coverages), the CH_3OH formation will proceeds via consecutive hydrogenation of C*-O fragments by adsorbed hydrogen atom on the catalyst surface to form intermediate species C*-OH, H-C*-OH, H_2C^*-OH and finally, methanol CH_3OH. This would be also consistent with the Langmuir–Hinshelwood mechanism.

However, at high pressure of H_2, the reaction pathway will follow the Eley–Rideal mechanism where adsorbed C*OH and HC*OH species react with molecules H_2 from the gas phase in the slow steps of the reaction (steps 3a-4a). The lower activation energies of these steps (3a-4a) compare to those of steps (3b-4b) and the negative values of reaction energies (−97.8 and −22.4 kJ mol^{-1} indicating an exothermic nature) calculated by our work correspond well to thermodynamic and kinetic nature of the studied reaction: methanol productivity and rate formation predominates at high pressure.

Generally, In the CO hydrogenation the main reactions which accompany with the methanol synthesis (R1) are the Fischer–Tropsch process (R2) and water–gas shift (WGS) reaction (R3):

$$CO + 2H_2 \rightleftharpoons CH_3OH \quad \text{(R1)}$$

$$(2n + 1)\ H_2 + n\ CO \rightarrow C_nH_{2n+2} + n\ H_2O \quad \text{(R2)}$$

$$CO + H_2O \rightleftharpoons CO_2 + H_2 \quad \text{(R3)}$$

These reactions are not independent, and any one of them can be expressed as a linear combination of the other two. Also conversion to methanol is limited by equilibrium of the reactions taking place. The synthesis of CH_3OH from syngas is a equilibrium limited process. It is a high-pressure and exothermic reaction. Increasing pressure results in the reaction of $CO+2H_2 \rightleftharpoons CH_3OH$ shifting towards the right hand side. On the other hand, the CO conversion, the hydrocarbon formation through Fischer–Tropsch (FT) reaction and the production of CO_2 from the WGS process significantly increase with increasing temperature, as a result the CH_3OH selectivity decreases. Therefore, it is necessary to conduct the ($2H_2$ + CO) reaction at high pressures rather than at high temperatures to obtain high CH_3OH yields.

Ding et al. [52] and Wu et al. [14] studied the kinetics of CO hydrogenation into methanol and found that at high temperature (>330 °C) the alcohol yield was not consistent with the conversion of CO because at these temperatures the hydrocarbon production is more selective and the WGS reaction becomes significant. The methanol selectivity monotonically decreased with increasing temperature. But increasing the pressure increases the selectivity of methanol, and higher alcohols.

Ladera et al. [53] investigated the hydrogenation of CO_2 into methanol over Ga-doped $Cu/ZnO/ZrO_2$ catalysts Their investigation shows that the CH_3OH yield is increased upon increasing the H_2 pressure but levels off with the CO_2 pressure. The authors suggested that CH_3OH formation obeys the Eley–Rideal mechanism whereby adsorbed CO_2 species (CO_2*) react with H_2 molecule in the slow step of the reaction.

4. Conclusions

In the present study, the elementary steps of CO hydrogenation leading to the formation of CH_3OH on Co_4/Al_2O_3 were analyzed using the density functional theory calculations. A 4-atom Co cluster, Co_4, was located on the Al_2O_3 (104) surface. The calculated results indicated that the formation of Co_4/Al_2O_3 systems is accompanied by the formation of chemical bonds between Co and O atoms. CO is more readily absorbed on Co_4/Al_2O_3 than on alone a Co_4 cluster. In the CO hydrogenation process, methanol was synthesized through the intermediates C*-OH, H-C*-OH, and H_2C*-OH:

$$H_2 \rightarrow H^* + H^*$$

$$H^*\text{-}H^* + C^*\text{-}O \rightarrow H^* + C^*\text{-}OH$$

$$H^* + C^*\text{-}OH \rightarrow H\text{-}C^*\text{-}OH$$

$$H_2 + H\text{-}C^*\text{-}OH \rightarrow H_2C^*\text{-}OH + H^*$$

$$H_2 + H_2C^*\text{-}OH \rightarrow H_3C\text{-}OH + H^*$$

Our calculations show that the formation of C*-O-H induced a significant change in the geometry of Co_4 and our calculated results show that the interaction between Al_2O_3 support and Co catalyst plays a key role in the catalytic hydrogenation of CO to methanol.

The studies have also suggested that the initial steps are kinetically difficult although the COH/HCOH pathway is slightly favored more than HCO/H_2CO pathway. CH_3OH synthesis on Co_4/Al_2O_3 proceeds through CO reaction with hydrogen via either an Eley–Rideal or Langmuir–Hinshelwood pathway to form C*O, C*OH, HC*OH, H_2C*OH and finally, methanol (CH_3OH), with both hydrogenation steps forming C*-OH and final product as rate-limiting.

Our DFT results shed light on the effects of Al_2O_3 support and the H_2 pressure on the reaction pathways for methanol formation from CO hydrogenation over a Co catalyst. The strong metal–support interaction will lead to high dispersion of active sites. This theoretical study allows us to describe CO hydrogenation reaction in detail and is capable of explaining the key experimental trend of this important but complex reaction.

Supplementary Materials: The following are available online at http://www.mdpi.com/2073-4344/9/1/6/s1, **Table S1**. The calculated energy (Ecluster) of Co4 clusters with different number of unpaired electrons. **Table S2**. The calculated interation energy (Eint) between Co4 cluster and Al_2O_3. **Table S3.** The calculated adsorption energies (E_{ads}) for the adsorption of CO on Co_4 and Co_4/Al_2O_3 systems. **Table S4.** The calculated adsorption energies (E_{ads}) for the adsorption of H_2 on Co_4 and Co_4/Al_2O_3 system. **Table S5.** The calculated adsorption energies (E_{ads}) for the adsorption of CO and H_2 on Al_2O_3 system. **Table S6.** Transition state structures of CO hydrogenation on Co4/Al_2O_3.

Author Contributions: Conceptualization, L.M.C. and N.N.H.; Methodology, N.N.H. and N.T.T.H.; Formal Analysis, L.M.C. and N.N.H.; Investigation, N.N.H., N.T.T.H. and N.B.L.; Data Curation, N.T.T.H. and N.B.L.; Writing-Original Draft Preparation, N.N.H. and N.T.T.H.; Writing-Review andEditing, L.M.C. and N.T.T.H.; Visualization, L.M.C. and N.T.T.H.; Project Administration, L.M.C.

Funding: This research was funded by the Vietnam Ministry of Education and Training, grant number B2015-17-69.

Conflicts of Interest: The authors declare no conflict of interest. The founding sponsors had no role in the design of the study; in the collection, analyses, or interpretation of data; in the writing of the manuscript; and in the decision to publish the results.

References

1. Surisetty, V.R.; Dalai, A.K.; Kozinski, J. Alcohols as alternative fuels: An overview. *Appl. Catal. A* **2011**, *404*, 1–11. [CrossRef]
2. Saeidi, S.; Amin, N.A.S.; Rahimpour, M.R. Hydrogenation of CO_2 to value-added products—A review and potential future developments. *J. CO2 Util.* **2014**, *5*, 66–81. [CrossRef]

3. Hu, B.; Yin, Y.; Liu, G.; Chen, S.; Tsang, S.C.E. Hydrogen spillover enabled active Cu sites for methanol synthesis from CO_2 hydrogenation over Pd doped CuZn catalysts. *J. Catal.* **2018**, *359*, 17–26. [CrossRef]
4. Abrol, S.; Hilton, C.M. Modeling, simulation and advanced control of methanol production from variable synthesis gas feed. *Comput. Chem. Eng.* **2012**, *40*, 117–131. [CrossRef]
5. Su, X.; Xu, J.; Liang, B.; Duan, H.; Hou, B.; Huang, Y. Catalytic carbon dioxide hydrogenation, to methane: A review of recent studies. *J. Energy Chem.* **2016**, *25*, 553–565. [CrossRef]
6. Weststrate, C.J.; van de Loosdrecht, J.; Niemantsverdriet, J.W. Spectroscopic insights into cobalt catalyzed Fischer-Tropsch synthesis: A review of the carbon monoxide interaction with single crystalline surfaces of cobalt. *J. Catal.* **2016**, *342*, 1–16. [CrossRef]
7. Liu, Y.; Murata, K.; Inaba, M.; Takahara, I.; Okabe, K. Mixed alcohols synthesis from syngas over Cs- and Ni-modified Cu/CeO_2 catalysts. *Fuel* **2013**, *104*, 62–69. [CrossRef]
8. Park, N.; Park, M.J.; Lee, Y.J.; Ha, K.S.; Jun, K.W. Kinetic modeling of methanol synthesis over commercial catalysts based on three-site adsorption. *Fuel Process. Technol.* **2014**, *125*, 139–147. [CrossRef]
9. Liu, Y.; Deng, X.; Han, P.; Huang, W. CO hydrogenation to higher alcohols over CuZnAl catalysts without promoters: Effect of pH value in catalyst preparation. *Fuel Process. Technol.* **2017**, *167*, 575–581. [CrossRef]
10. Bai, Y.; He, D.; Ge, S.; Liu, H.; Liu, J.; Huang, W. Influences of preparation methods of ZrO_2 support and treatment conditions of Cu/ZrO_2 catalysts on synthesis of methanol via CO hydrogenation. *Catal. Today* **2010**, *149*, 111–116. [CrossRef]
11. Studt, F.; Abild-Pedersen, F.; Wu, Q.; Jensen, A.D.; Temel, B.; Grunwaldt, J.D.; Nørskov, J.K. CO hydrogenation to methanol on Cu–Ni catalysts: Theory and experiment. *J. Catal.* **2012**, *293*, 51–60. [CrossRef]
12. Chai, S.H.; Schwartz, V.; Howe, J.Y.; Wang, X.; Kidder, M.; Overbury, S.H.; Dai, S.; Jiang, D.E. Graphitic mesoporous carbon-supported molybdenum carbides for catalytic hydrogenation of carbon monoxide to mixed alcohols. *Microporous Mesoporous Mater.* **2013**, *170*, 141–149. [CrossRef]
13. Surisetty, V.R.; Eswaramoorthi, I.; Dalai, A.K. Comparative study of higher alcohols synthesis over alumina and activated carbon-supported alkali-modified MoS_2 catalysts promoted with group VIII metals. *Fuel* **2012**, *96*, 77–84. [CrossRef]
14. Wu, Q.; Christensen, J.M.; Chiarello, G.L.; Duchstein, L.D.; Wagner, J.B.; Temel, B.; Grunwaldt, J.D.; Jensen, A.D. Supported molybdenum carbide for higher alcohol synthesis from syngas. *Catal. Today* **2013**, *215*, 162–168. [CrossRef]
15. Andersen, A.; Kathmann, S.M.; Lilga, M.A.; Albrecht, K.O.; Hallen, R.T.; Mei, D. Effects of potassium doping on CO hydrogenation over MoS_2 catalysts: A first-principles investigation. *Catal. Commun.* **2014**, *52*, 92–97. [CrossRef]
16. Gnanamani, M.K.; Jacobs, G.; Keogh, R.A.; Shafer, W.D.; Sparks, D.E.; Hopps, S.D.; Thomas, G.A.; Davis, B.H. Fischer-Tropsch synthesis: Effect of pretreatment conditions of cobalt on activity and selectivity for hydrogenation of carbon dioxide. *Appl. Catal. A* **2015**, *499*, 39–46. [CrossRef]
17. Wang, P.; Zhang, J.; Bai, Y.; Xiao, H.; Tian, S.; Xie, H.; Yang, G.; Tsubaki, N.; Han, Y.; Tan, Y. Ternary copper–cobalt–cerium catalyst for the production of ethanol and higher alcohols through CO hydrogenation. *Appl. Catal. A* **2016**, *514*, 14–23. [CrossRef]
18. Du, H.; Zhu, H.; Liu, T.; Zhao, Z.; Chen, X.; Dong, W.; Lu, W.; Luo, W.; Ding, Y. Higher alcohols synthesis via CO hydrogenation on Fe-promoted Co/AC catalysts. *Catal. Today* **2017**, *281*, 549–558. [CrossRef]
19. Nikparsaa, P.; Mirzaeia, A.A.; Atashib, H. Effect of reaction conditions and Kinetic study on the Fischer-Tropsch synthesis over fused Co Ni/Al_2O_3 catalyst. *J. Fuel Chem. Technol.* **2014**, *42*, 710–718. [CrossRef]
20. Zhang, Y.; Sun, Q.; Deng, J.; Wu, D.; Chen, S. A high activity $Cu/ZnO/Al_2O_3$ catalyst for methanol synthesis: Preparation and catalytic properties. *Appl. Catal. A* **1997**, *158*, 105–120. [CrossRef]
21. Li, D.; Yang, C.; Li, W.; Sun, Y.; Zhong, B. Ni/ADM: A high activity and selectivity to $C_{2+}OH$ catalyst for catalytic conversion of synthesis gas to C_1-C_5 mixed alcohols. *Top. Catal.* **2005**, *32*, 233–239. [CrossRef]
22. Shi, X.R.; Jiao, H.; Hermann, K.; Wang, J. CO hydrogenation reaction on sulfided molybdenum catalysts. *J. Mol. Catal. A Chem.* **2009**, *312*, 7–17. [CrossRef]
23. Díez-Ramírez, J.; Sánchez, P.; Kyriakou, V.; Zafeiratos, S.; Marnellos, G.E.; Konsolakis, M.; Dorado, F. Effect of support nature on the cobalt-catalyzed CO_2 hydrogenation. *J. CO2 Util.* **2017**, *21*, 562–571. [CrossRef]
24. Zuo, Z.J.; Han, P.D.; Li, Z.; Hu, J.S.; Huang, W. Can methanol be synthesized from CO by direct hydrogenation over Cu/ZnO catalysts? *Appl. Surf. Sci.* **2012**, *261*, 640–646. [CrossRef]

25. Lee, J.H.; Reddy, K.H.; Jung, J.S.; Yang, E.H.; Moon, D.J. Role of support on higher alcohol synthesis from syngas. *Appl. Catal. A* **2014**, *480*, 128–133. [CrossRef]
26. Medford, A.J.; Sehested, J.; Rossmeisl, J.; Chorkendorff, I.; Studt, F.; Nørskov, J.K.; Moses, P.G. Thermochemistry and micro-kinetic analysis of methanol synthesis on ZnO (0001). *J. Catal.* **2014**, *309*, 397–407. [CrossRef]
27. Prasad, P.S.; Bae, J.; Jun, K.-W.; Lee, K.-W. Fischer–Tropsch Synthesis by Carbon Dioxide Hydrogenation on Fe-Based Catalysts. *Catal. Surv. Asia* **2008**, *12*, 170–183. [CrossRef]
28. Reuel, R.C.; Bartholomew, C.H. Effects of support and dispersion on the CO hydrogenation activity/selectivity properties of cobalt. *J. Catal.* **1984**, *85*, 78–88. [CrossRef]
29. Zhao, Y.; Rousseau, R.; Li, J.; Mei, D. Theoretical study of syngas hydrogenation to methanol on the polar Zn-terminated ZnO (0001) surface. *J. Phys. Chem. C* **2012**, *116*, 15952–15961. [CrossRef]
30. Reimers, W.; Zubieta, C.; Baltan'as, M.A.; Branda, M.M. A DFT Approach for Methanol Synthesis via Hydrogenation of CO on Gallia, Ceria and ZnO surfaces. *Appl. Surf. Sci.* **2018**, *436*, 1003–1017. [CrossRef]
31. Liuan, P.; Yang, Y.; White, M.G. Theoretical perspective of alcohol decomposition and synthesis from CO_2 hydrogenation. *Surf. Sci. Rep.* **2013**, *68*, 233–272. [CrossRef]
32. Dou, M.; Zhang, M.; Chen, Y.; Yu, Y. Theoretical Study of Methanol Synthesis from CO_2 and CO Hydrogenation on the surface of ZrO_2 supported In_2O_3 catalyst. *Surf. Sci.* **2018**, *672–673*, 7–12. [CrossRef]
33. Zha, H.; Dong, X.; Yu, Y.; Zhang, M. Hydrogen-assisted versus Hydroxyl-assisted CO Dissociation over Co-doped Cu(111): A DFT Study. *Surf. Sci.* **2018**, *669*, 114–120. [CrossRef]
34. Pan, Y.X.; Liu, C.J.; Ge, Q. Effect of surface hydroxyls on selective CO_2 hydrogenation over Ni_4/γ-Al_2O_3: A density functional theory study. *J. Catal.* **2010**, *272*, 227–234. [CrossRef]
35. Zhang, R.G.; Wang, B.J.; Liu, H.Y.; Ling, L.X. Effect of surface hydroxyls on CO_2 hydrogenation over Cu/γ–Al_2O_3 catalyst: A theoretical study. *J. Phys. Chem. C* **2011**, *115*, 19811–19818. [CrossRef]
36. Zuo, Z.J.; Wang, L.; Han, P.D.; Huang, W. Methanol synthesis by CO and CO_2 hydrogenation on Cu/γ-Al_2O_3 surface in liquid paraffin solution. *Appl. Surf. Sci.* **2014**, *290*, 398–404. [CrossRef]
37. Yang, Z.; Yu, J.; Li, C.; Zhong, Y.; Xuan, W.; Ren, Z.; Wang, Q.; Dai, Y.; Wang, H. Preparation of textured porous Al_2O_3 ceramics by slip casting in a strong magnetic field and its mechanical properties. *Cryst. Res. Technol.* **2015**, *50*, 645–653. [CrossRef]
38. Soler, J.M.; Artacho, E.; Gale, J.D.; García, A.; Junquera, J.; Ordejón, P.; Sánchez-Portal, D. The SIESTA method for ab initio order-N materials simulation. *J. Phys. Condens. Matter* **2002**, *14*, 2745–2779. [CrossRef]
39. Cheng, J.; Hu, P.; Ellis, P.; French, S.; Kelly, G.; Lok, C.M. A DFT study of the chain growth probability in Fischer-Tropsch synthesis. *J. Catal.* **2008**, *257*, 221–228. [CrossRef]
40. Cheng, J.; Hu, P.; Ellis, P.; French, S.; Kelly, G.; Lok, C.M. Chain growth mechanism in Fischer-Tropsch synthesis: A DFT study of C-C coupling over Ru, Fe, Rh, and Re surfaces. *J. Phys. Chem. C* **2008**, *112*, 6082–6086. [CrossRef]
41. Cheng, J.; Gong, X.Q.; Hu, P.; Lok, C.M.; Ellis, P.; French, S. A quantitative determination of reaction mechanisms from density functional theory calculations: Fischer–Tropsch synthesis on flat and stepped cobalt surfaces. *J. Catal.* **2008**, *254*, 285–295. [CrossRef]
42. Perdew, J.P.; Burke, K.; Ernzerhof, M. Generalized Gradient Approximation Made Simple. *Phys. Rev. Lett.* **1996**, *77*, 3865–3868. [CrossRef] [PubMed]
43. Hamann, D.R.; Schlüter, M.; Chiang, C. Norm-conserving pseudopotentials. *Phys. Rev. Lett.* **1979**, *43*, 1494–1497. [CrossRef]
44. Henkelman, G.; Uberuaga, B.P.; Jónsson, H. A climbing image nudged elastic band method for finding saddle points and minimum energy paths. *J. Chem. Phys.* **2000**, *133*, 9901–9904. [CrossRef]
45. Fonseca Guerra, C.; Handgraaf, J.-W.; Baerends, E.J.; Bickelhaupt, F.M. Voronoi deformation density (VDD) charges: Assessment of the Mulliken, Bader, Hirshfeld, Weinhold, and VDD methods for charge analysis. *J. Comput. Chem.* **2004**, *25*, 189–210. [CrossRef]
46. Slater, J.C. Atomic Radii in Crystals. *J. Chem. Phys.* **1964**, *41*, 3199–3205. [CrossRef]
47. Fielicke, A.; Gruene, P.; Meijer, G.; Rayner, D.M. The adsorption of CO on transition metal clusters: A case study of cluster surface chemistry. *Surf. Sci.* **2009**, *603*, 1427–1433. [CrossRef]
48. Huber, K.P.; Herzberg, G. *Molecular Spectra and Molecular Structure, IV. Constants of Diatomic Molecules*; Van Nostrand Reinhold Company: New York, NY, USA, 1979.
49. Cottrell, T.L. *The Strengths of Chemical Bonds*, 2nd ed.; Butterworths: London, UK, 1958.

50. Nordlander, P.; Holloway, S.; Nørskov, J.K. Hydrogen adsorption on metal surfaces. *Surf. Sci.* **1984**, *136*, 59–81. [CrossRef]
51. Ferrin, P.; Kandoi, S.; Nilekar, A.U.; Mavrikakis, M. Hydrogen adsorption, absorption and diffusion on and in transition metal surfaces: A DFT study. *Surf. Sci.* **2012**, *606*, 679–689. [CrossRef]
52. Ding, M.; Qiu, M.; Liu, J.; Li, Y.; Wang, T.; Ma, L.; Wu, C. Influence of manganese promoter on co-precipitated Fe–Cu based catalysts for higher alcohols synthesis. *Fuel* **2013**, *109*, 21–27. [CrossRef]
53. Ladera, R.; Pérez-Alonso, F.J.; González-Carballo, J.M.; Ojeda, M.; Rojas, S.; Fierro, J.L.G. Catalytic valorization of CO_2 via methanol synthesis with Ga-promoted Cu–ZnO–ZrO_2 catalysts. *Appl. Catal. B Environ.* **2013**, *142–143*, 241–248. [CrossRef]